Electrical transport and thermoelectric properties of $Y_{1-x}Ca_xCoO_3$ ($0 \leqslant x \leqslant 0.1$) at high temperatures

Y. Liu, X. Y. Qin,[a] H. X. Xin, J. Zhang, and H. J. Li
Key Laboratory of Materials Physics, Institute of Solid State Physics, Chinese Academy of Sciences, 230031 Hefei, People's Republic of China

Y. F. Wang
Department of Applied Chemistry, Graduate School of Engineering, Nagoya University, Furo-cho Chikusa, Nagoya 464-8603 Japan

(Received 20 September 2006; accepted 25 February 2007; published online 30 April 2007)

The effects of Ca substitution for Y on the electrical transport and thermoelectric properties of $Y_{1-x}Ca_xCoO_3$ ($0 \leqslant x \leqslant 0.1$), prepared by using the sol-gel process, were investigated in the temperature range from 300 to 780 K. The results indicated that direct current electrical resistivity ρ of $Y_{1-x}Ca_xCoO_3$ decreased remarkably with increasing Ca content x as $x \leqslant 0.01$, which could mainly be attributed to the increase of hole concentration due to substitution of Ca^{2+} for Y^{3+}. The temperature dependences of the resistivity for $Y_{1-x}Ca_xCoO_3$ were all found to be basically consistent with small-polaron hopping conduction model. Although Seebeck coefficient S of $Y_{1-x}Ca_xCoO_3$ at low temperatures $T < \sim 550$ K decreased remarkably with increasing x, it approached a limit value ~ 150 μV/K at ~ 800 K for all the samples with different x, which was consistent well with the thermopower resulting from the degeneracy of electron configuration estimated from Heikes formula by assuming that Co^{3+} and Co^{4+} exist in low spin state. Experiments showed that thermal conductivity κ of $Y_{1-x}Ca_xCoO_3$ came mainly from its lattice component, whose decrease with increasing x could be chiefly ascribed to impurity-scattering effect due to Ca doping. The thermoelectric figure of merit ZT ($=S^2T/\rho\kappa$) of $Y_{1-x}Ca_xCoO_3$ changed nonmonotonously with increasing doping content of Ca, and $Y_{0.95}Ca_{0.05}CoO_3$ was found to have optimum thermoelectric properties with $ZT=0.019$ at 660 K, which was about ten-fold greater than that of $YCoO_3$, indicating that its thermoelectric properties could be improved effectively by appropriate substitution of Ca for Y in this compound. © *2007 American Institute of Physics*.
[DOI: 10.1063/1.2721381]

I. INTRODUCTION

Oxide thermoelectric materials have attracted broad interests in recent several years due to their notably potential applications in "environmentally friendly" power generation from vast waste heat.[1–6] The evaluation of thermoelectric properties for these oxide materials can be characterized by a dimensionless figure of merit[7] ZT, i.e., $ZT=PT/\kappa$, where $P=S^2/\rho$ (S, Seebeck coefficient or thermopower; ρ, electrical resistivity) is the power factor related to electrical property,[8] T and κ are absolute temperature and thermal conductivity, respectively. Therefore, it is necessary for a high performance thermoelectric material to possess large power factor, and relatively low thermal conductivity.

Since Terasaki *et al.*[9] found that the layered single crystal $NaCo_2O_4$ exhibited a high thermopower and low electrical resistivity in 1997, layered cobalt based oxide thermoelectric materials have been investigated widely.[10–19] Recently, Androulakis *et al.*[20] reported that perovskite-type cobalt based oxide $La_{0.95}Sr_{0.05}CoO_3$ was an efficient room-temperature thermoelectric material: its ZT at room temperature arrived at about 0.9. This kind of cobalt-based oxide has many advantages as thermoelectric materials. For instance, they have fairly large thermopower in the vicinity of room temperature [e.g., $S_{300\ K} \sim 640$ $\mu V\ K^{-1}$ for $LaCoO_3$,[21] $S_{300\ K} \sim 1300$ $\mu V\ K^{-1}$ for $HoCoO_3$,[22] and $S_{300\ K} \sim 1050$ $\mu V\ K^{-1}$ for $YCoO_3$ (Ref. 23), and so forth] and small thermal conductivity [for example, $\kappa=3.0$ W m^{-1} K^{-1} at 300 K for $La_{0.95}Sr_{0.05}CoO_3$ (Ref. 20)]. In addition, they possess high thermal stability, oxidation resistance, and nontoxicity compared to the traditional thermoelectric materials, e.g., PbTe, Bi_2Te_3, etc.

Demazeau *et al.*[24] synthesized $YCoO_3$ oxide, which is a distorted perovskite structure[25] with orthorhombic symmetry [space group *Pbnm* ($Z=4$)], where six oxygen atoms surround each cobalt ion, and there is only one form of cobalt site. It was once investigated widely for its interesting electrical and magnetic transport properties.[13,26] However, no systemic investigations on high-temperature thermoelectric properties of Ca doped $YCoO_3$ were reported at present.[27,28] In this paper, we reported the investigations on dc electrical resistivity and thermoelectric properties of $Y_{1-x}Ca_xCoO_3$ ($0 \leqslant x \leqslant 0.1$) in high temperature range from 300 to 780 K.

II. EXPERIMENTAL PROCEDURES

Calcium doped yttrium cobaltites were synthesized from stoichiometric amounts of yttrium, calcium, and cobalt nitrates. $0.05x$ ($x=0, 0.01, 0.05, 0.1$) mol of $Ca(NO_3)_2 \cdot 4H_2O$

[a]Author to whom correspondence should be addressed; electronic mail: xyqin@issp.ac.cn

TABLE I. List of room-temperature lattice parameters (a, b, and c), Goldschmidt tolerance factor t, theory density d_{the}, measured density d_{mea}, and relative density d_{rel} for $Y_{1-x}Ca_xCoO_3$.

x	a (Å)	b (Å)	c (Å)	t	d_{the} (g cm^{-3})	d_{mea} (g cm^{-3})	d_{rel} (%)
0.00	5.1393	5.4197	7.4588	0.8014	6.2614	5.6507	90.2
0.01	5.1400	5.4181	7.4580	0.8018	6.2475	5.6313	90.1
0.05	5.1455	5.4162	7.4619	0.8032	6.1773	5.4580	88.4
0.10	5.1468	5.4133	7.4593	0.8050	6.1032	5.5081	90.3

(99.0%), $0.05(1-x)$ mol of $Y(NO_3)_3\cdot 6H_2O$ (99.0%), and 0.05 mol of $Co(NO_3)_2\cdot 6H_2O$ (99.0%) were dissolved in 50 ml of an aqueous solution of 0.05M (mol/l) citric acid (99.5%) confected by deionized water. The solutions were continuously stirred for about 1 h resulting in a homogenization of Y^{3+}, Ca^{2+}, and Co^{2+} cations in the mixture solution. Subsequently, the mixtures were slowly heated to 90 °C, and at this temperature they were dried for 12 h, forming a brown powder from the mixtures. The brown powders were calcined in air at atmospheric pressure in muffle furnace at 300 °C for 2 h, forming black powder samples. Then, these powder samples were grinded and subsequently compressed into pellets with 13 cm in diameter. Finally, bulk samples were obtained by sintering the green pellets in air in tube furnace at 900 °C for 120 h, followed by spontaneous cooling slowly down to room temperature in the furnace. To investigate the effect of possible oxygen deficiency in the synthesized samples, some green pellets were sintered in air for 24 h and then annealed at 900 °C in oxygen flow (10 ml min^{-1}) in tube furnace for 2 h, and compare their electrical transport properties before and after annealing.

The accurate lattice parameters at room temperature were determined from the d value of the x-ray diffraction (XRD) peaks (obtained from Philips-X'Pert PRO diffractometer with Cu K_α irradiation) using a standard least-squares refinement method with a Si standard for calibration. To measure their properties, bar-shaped specimens of the size $(\sim)12\times(\sim)2\times(\sim)1$ mm^3, were cut from the bulk samples. The electrical resistivity and Seebeck coefficient were measured on a computer-assisted device. The electrical resistivities were measured in vacuum by a conventional standard dc four-probe method at the temperatures from 300 to 720 K. Seebeck coefficient was also measured in vacuum in the temperature range from 300 to 780 K. The bulk sample densities were measured by using Achimedes method with an accuracy of ±1.5%. Heat capacity was measured by differential scanning calorimetry (DSC-2910 thermal analyzer instruments) at the heating rate of 2 °C min^{-1} in vacuum and calibrated by a standard sapphire sample measured under the same condition. Thermal diffusivity was determined by laser-flash method (ULVAC-TC3000V), in which disk-shaped samples with diameter of about 10 mm and thickness of about 1 mm were used. The thermal conductivity κ was obtained from multiplication of thermal diffusivity by specific heat capacity and bulk density.

III. RESULTS AND DISCUSSION

A. Microstructure characterization

The XRD experiments confirmed that the crystalline structure of the doped $Y_{1-x}Ca_xCoO_3$ compounds ($x\neq 0$) is the same as that of pristine compound[29] $YCoO_3$. However, accurate measurements of lattice constants showed that the lattice parameters of $Y_{1-x}Ca_xCoO_3$ changed with increasing Ca content, as listed in Table I. One can see from Table I that the lattice parameter a increases from 5.1393 to 5.1468 Å with increasing Ca content x from 0 to 0.10; while the lattice parameter b decreases from 5.4197 Å for $x=0$ to 5.4133 Å for $x=0.1$. This result indicates the substitution of Ca for Y in $YCoO_3$ has occurred. Due to this change in lattice constants, the volume of unit cell of $Y_{1-x}Ca_xCoO_3$ changed accordingly. Furthermore, because of the substitution of Ca with smaller atomic mass for Y with greater atomic mass, the total atomic weight per unit cell will change. Based on values of both lattice constants and total atomic weights per unit cell of $Y_{1-x}Ca_xCoO_3$ with different Ca contents, the theoretical density d_{the} for all the samples with different Ca contents were estimated, as listed also in Table I. One can see that with increasing Ca content, the density d_{the} of $Y_{1-x}Ca_xCoO_3$ decreases slightly. Table I also lists experimentally measured density d_{mea} of every $Y_{1-x}Ca_xCoO_3$ (polycrystalline) bulk sample. It can be seen that the relative density d_{rel} of all the samples is around 88%–90%, which indicates that densification state of all the samples are almost the same within the experimental error. This result suggests that the microstructural differences (porosity) among the samples have negligible effects on revealing the intrinsic transport properties (electrical and thermal conductivity) of different $Y_{1-x}Ca_xCoO_3$ samples (with different x).

In order to describe the deformation degree, a geometrical quantity, Goldschmidt tolerance factor t is introduced here, which is a fundamental parameter characterizing the degree of structural distortion in perovskites with the general formula ABO_3. It is defined as[30]

$$t=\frac{r_A+r_O}{\sqrt{2}(r_B+r_O)}, \tag{1}$$

where r_A, r_B, and r_O represent the average ionic radii of the respective cations (A and B) and oxygen, respectively. The tolerance factor t measured for $Y_{1-x}Ca_xCoO_3$ is listed in Table I. One can see that for all $Y_{1-x}Ca_xCoO_3$ samples the relation $a<c/\sqrt{2}<b$ exists, which means they belong to so-called O-type structure,[23] indicating that the deformation of lattice in $YCoO_3$ is relatively small after Ca substitution for Y. The dominating source of orthorhombic small distortion comes from buckling of the octahedral CoO_6 network, as suggested elsewhere.[23] One also notes from Table I that with increasing x the tolerance factor t increases, which suggests that bucking of octahedral network becomes smaller as x increases.[23] Since the average ionic radius of B and O is invariable in our condition investigated, the decrease in lat-

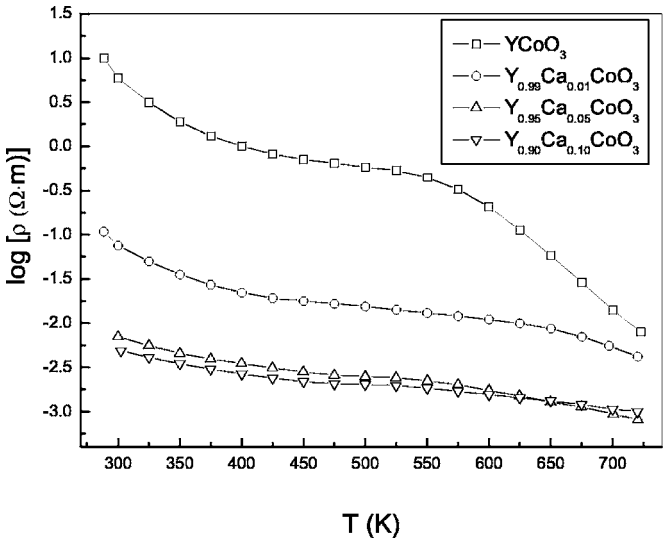

FIG. 1. Electrical resistivity ρ as a function of temperature T for $Y_{1-x}Ca_xCoO_3$ (x=0, 0.01, 0.05, 0.1).

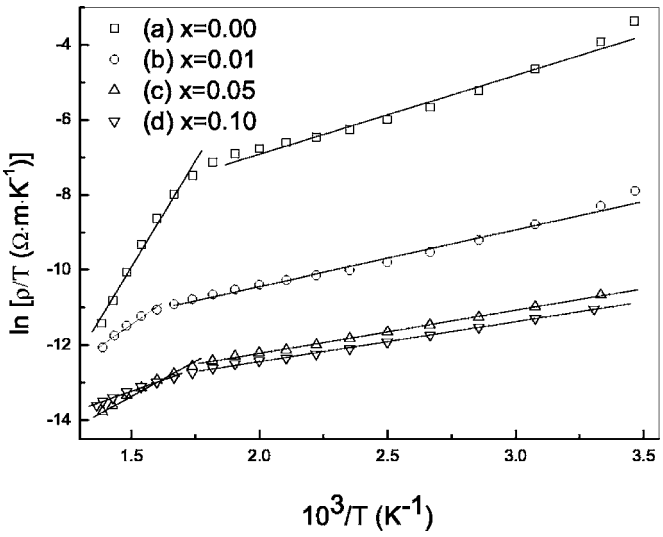

FIG. 2. Plot of $\ln(\rho/T)$ vs $1/T$ for $Y_{1-x}Ca_xCoO_3$ (x=0, 0.01, 0.05, 0.1) with (a) x=0, (b) x=0.01, (c) x=0.05, and (d) x=0.1. The solid lines are the best fit of the experimental data to formula (2).

tice distortion is actually caused by the partial substitution of Ca for Y, and this change of lattice distortion would affect the transport properties of $Y_{1-x}Ca_xCoO_3$ (see following sections).

B. Resistivity and its temperature dependences

The temperature dependences of dc electrical resistivity ρ in the form of $\log \rho$ for the $Y_{1-x}Ca_xCoO_3$ ($0 \leqslant x \leqslant 0.1$) oxides in the temperature range from 300 to 720 K are shown in Fig. 1. One can see that the resistivity of $Y_{1-x}Ca_xCoO_3$ ($x>0$) decreases remarkably with increasing Ca content of doping. For example, the resistivity at 400 K decreases rapidly from about 1.0 Ω m for x=0 to ~2.2 $\times 10^{-2}$ Ω m for x=0.01, and to ~3.5×10^{-3} Ω m for x =0.05; then it decreases slowly to ~2.7×10^{-3} Ω m for x =0.10. Present results of the resistivity measurements are basically in agreement with the previous results reported for $Y_{1-x}Ca_xCoO_3$ by Hejtmanek *et al.*[27,28] (who only investigated the compounds with x=0, 0.1, and 0.2). The monotonous decrease of the resistivity could be related to the changes of both carrier (holes, as shown by measurements of thermopower in Fig. 5 and Hall coefficient measurements[29]) concentration and band structure after Ca substitution. As shown in Ref. 29, the hole concentration increased remarkably from ~10^{14} cm^{-3} for x=0 to ~10^{16} cm^{-3} for x=0.01 and then to ~10^{18} cm^{-3} for x=0.05. Then, hole concentration did not change obviously with further increase of Ca content, which indicates that the changing behavior of the carrier concentration with doping content is basically in agreement with that of the resistivity. In addition, the decrease in distortion of $Y_{1-x}Ca_xCoO_3$ after substitution of Ca^{2+} for Y^{3+} (as manifested by increasing the value of t) could have also some contribution to the decrease in the electrical resistivity because the decrease in the distortion will lead the average Co($3d$)-O($2p$)-Co($3d$) bond angle to tend to move towards 180°, making the Co($3d$)-O($2p$) orbit overlap become larger and interactions become stronger. This explanation was also advocated by He *et al.* in the similar system $La_{1-x}A_xCoO_3$ (A=Pb, Na).[31]

The electrical resistivity of $Y_{1-x}Ca_xCoO_3$ decreases with increasing temperature in the whole temperature range measured, i.e., $d\rho/dT/<0$, showing semiconductorlike behavior (Fig. 1). This phenomenon is also observed in other similar oxides, such as $La_{1-x}Sr_xCoO_3$.[21] In order to understand the conduction mechanism, we adopted several models (or laws) to fit the data of $Y_{1-x}Ca_xCoO_3$, viz. thermally activated conduction (TAC) model,[32] three dimensional (3D) Mott's variable range hopping (VRH) model,[32] and the adiabatic small polaron hopping conduction (SPHC) model,[33]

$$\rho(T) = \frac{1}{ne\mu} = \frac{T}{C}\exp\left(\frac{E_p}{k_B T}\right), \tag{2}$$

where n is the carrier concentration, e the electrical charge of carrier, μ the carrier mobility, $C=nea^2A$ (a the intersite distance, A the preexponential term related to the carrier scattering mechanism) approximately a constant, E_p the activation energy for polaron hopping, and k_B the Boltzmann constant. It is found that $\rho(T)$ follows the SPHC model very well in describing the transport of the carriers from the viewpoint of the fitting results of $\rho(T)$ data, as seen from the plots of $\ln(\rho/T)$ vs $1/T$ in Fig. 2, suggesting that the temperature dependences of the resistivity for $Y_{1-x}Ca_xCoO_3$ are consistent with the characteristics of well-accepted small-polaron hopping conduction. However, one also notes from Fig. 2 that for every sample there are two temperature regimes, within which the experimental data can be basically fitted with straight lines, but they exhibit different slopes at different temperature ranges. In other words, there is an obvious transition at ~$500<T<$~650 K for each of $Y_{1-x}Ca_xCoO_3$ sample.

On the other hand, the hopping activation energy E_{p1} in low temperature range (LTR) and E_{p2} in high temperature range (HTR) can be obtained by fitting the experimental data to formula (2) (see Fig. 2), as shown in Fig. 3. One can see

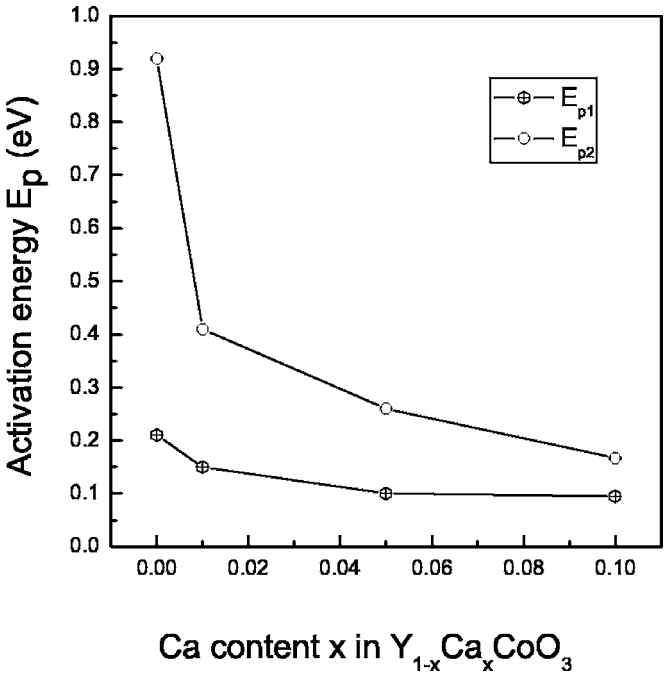

FIG. 3. Activation energy E_p vs Ca content of doping x in low-temperature (E_{p1}) and high-temperature (E_{p2}) regions for $Y_{1-x}Ca_xCoO_3$ ($x=0, 0.01, 0.05, 0.1$).

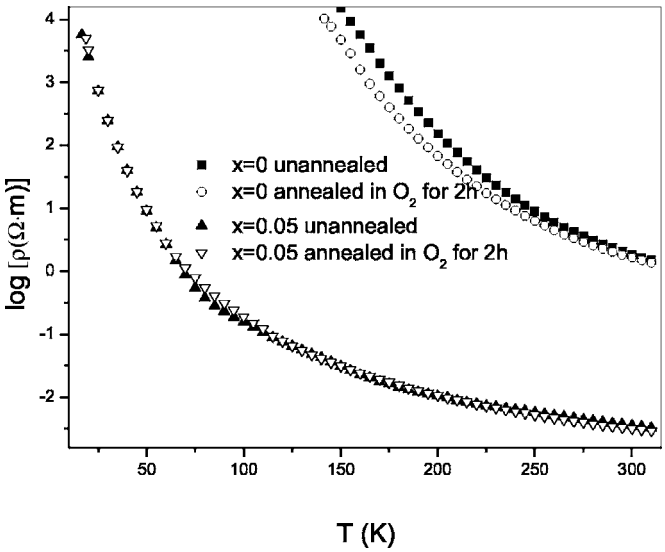

FIG. 4. Typical plots of log ρ vs temperature T for the $Y_{1-x}Ca_xCoO_3$ with $x=0$ and 0.05 unannealed and annealed in oxygen.

from Fig. 3 that the activation energy E_{p1} and E_{p2} all decrease with increasing content of Ca substitution: E_{p1} decreases monotonously from 0.21 eV for $x=0$ to 0.095 eV for $x=0.10$; while E_{p2} drops rapidly from 0.92 eV for $x=0$ to 0.41 eV for $x=0.01$, then it decreases to around 0.17 eV as x increases further to 0.10. The monotonous decrease of the activation energies indicates that the transport of the polarons becomes easier [being consistent with reduction in the resistivity (Fig. 1)] with increasing doping content of Ca, which would be associated with the decrease in distortion of $Y_{1-x}Ca_xCoO_3$ lattice (as manifested by increasing the value of t) after substitution of Ca^{2+} for Y^{3+}. However, one can see that as Ca doping content $x>0.05$, the decrease of the activation energies become slower, suggesting that much higher doping content ($x>0.1$, for instance) is not very effective to affecting the electrical transport properties.

As mentioned above, the decrease of the resistivity of $Y_{1-x}Ca_xCoO_3$ may mainly be related to the increase in hole concentration. The origin of the increase of hole concentration can be understood considering transition of oxidation state of cobalt caused by Ca substitution. The following reaction would occur upon Ca doping (in terms of Kröger-Vink notation[34]):

$$\mathrm{CaO} + \frac{1}{4}\mathrm{O_2} + (\mathrm{Y}_{\mathrm{Y}^{3+}}^{3+})^x + (\mathrm{Co}_{\mathrm{Co}^{3+}}^{3+})^x = (\mathrm{Ca}_{\mathrm{Y}^{3+}}^{2+})' + (\mathrm{Co}_{\mathrm{Co}^{3+}}^{4+})^{\cdot} + \frac{1}{2}\mathrm{Y_2O_3}, \quad (3)$$

where $(Y_{Y^{3+}}^{3+})^x$ denotes that Y^{3+} is sited on Y site, $(Co_{Co^{3+}}^{3+})^x$ that Co^{3+} is sited on Co site, $(Ca_{Y^{3+}}^{2+})'$ that Ca^{2+} is sited on Y site, and $(Co_{Co^{3+}}^{4+})^{\cdot}$ that Co^{4+} is sited on Co site. In stoichiometric $YCoO_3$, the charge states of Y and Co can be both expected to be +3. According to Eq. (3), when $YCoO_3$ is doped with Ca, Ca^{2+} ions substituting Y^{3+} ions will occur, i.e., appearance of $(Ca_{Y^{3+}}^{2+})'$. Therefore, the excess negative charges in the lattice are introduced due to the substitution of Ca^{2+} for Y^{3+}. In order to keep electroneutrality condition,[35] either the charge state of Co ions changes from Co^{3+} to Co^{4+} or oxygen vacancies are created. The $(Co_{Co^{3+}}^{4+})^{\cdot}$ species thus formed can be considered to be holes, contributing to electrical conduction. It was reported[20] that the Co ions at room temperature exist mostly as Co^{3+} in $YCoO_3$, which leads to rather large resistivity [6.9 Ω m at 300 K (Ref. 29)]. As shown in formula (3), with increasing Ca content of substitution the number of Co^{4+} ions and so the concentration of $(Co_{Co}^{Co^{4+}})^{\cdot}$ increase, which will lead to a decrease in resistivity of $Y_{1-x}Ca_xCoO_3$. Of course, if substantial oxygen vacancies were formed upon doping the hole concentration in $Y_{1-x}Ca_xCoO_3$ will also increase. To examine the oxygen vacancy effect, electrical resistivity of samples only sintered in air and those sintered in air and then annealed in oxygen were measured and compared with one another. As a typical example, Fig. 4 gives the plots of log ρ versus temperature T for the $Y_{1-x}Ca_xCoO_3$ with $x=0$ and 0.05 annealed and unannealed in oxygen. It can be seen that for the sample with $x=0$ annealing in oxygen has very limited influences on its resistivity below room temperature. In contrast, the annealing affects hardly the resistivity of $Y_{1-x}Ca_xCoO_3$ with $x=0.05$ in the whole temperature investigated. Obviously, if there are appreciable number of oxygen vacancies produced by doping, annealing in oxygen will eliminate these vacancies more or less, which should lead to pronounced changes (increase) of its resistivity. Hence, the fact that resistivity of $Y_{1-x}Ca_xCoO_3$ ($x\neq 0$) is hardly affected by annealing in oxygen suggests that the effects of possible oxygen vacancies produced by doping on the electrical transport properties of $Y_{1-x}Ca_xCoO_3$ is negligibly small, as compared to $(Co_{Co^{3+}}^{4+})^{\cdot}$ species.

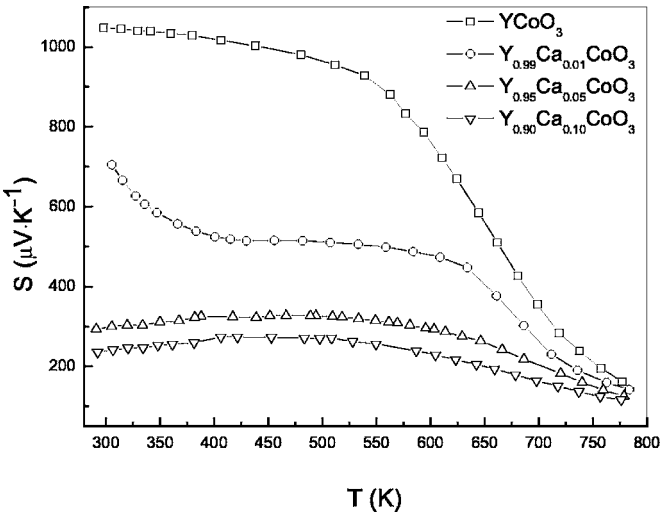

FIG. 5. Seebeck coefficient S as a function of temperature T for $Y_{1-x}Ca_xCoO_3$ (x=0, 0.01, 0.05, 0.1).

C. Thermoelectric properties

1. Thermopower

The temperature dependences of Seebeck coefficient (S) for the $Y_{1-x}Ca_xCoO_3$ ($0 \leqslant x \leqslant 0.1$) oxides in the temperature range from 300 to 780 K are presented in Fig. 5. The sign of the Seebeck coefficient is positive throughout the whole temperature range measured for all the oxides, indicating that major carriers in these samples are holes, in agreement with Hall measurements.[29] As temperature increases from 300 to ~550 K, the Seebeck coefficient for $YCoO_3$ decreases slowly from ~1048 to ~906 $\mu V\,K^{-1}$, then it decreases rapidly to ~191 $\mu V\,K^{-1}$ as temperature increases further to 760 K. The temperature behavior of S obtained here for $YCoO_3$ are basically consistent with those reported previously for $YCoO_3$ by several other authors.[23,27,28] But, the magnitude of S obtained here is a little bit larger than that reported by Hejtmanek *et al.*[27,28] This difference may be caused by different fabrication methods [solid-state reaction (used by them) versus sol-gel process (used here)] and/or compositions of the raw materials used by different authors, for the electronic properties of semiconductinglike $YCoO_3$ are very sensitive to synthesis process (which affects oxygen vacancies present, for instance) and impurity content. The rapid decrease of S at $T > \sim 550$ K could be attributed to transition from semiconducting state to metallic state for $RCoO_3$ system (R=La, Nd, Sm, Eu, Gd, Ho, and Y),[26,36] although the mechanism of this transition is a controversy issue.[26,36] Moreover, it could be seen from Fig. 5 that Seebeck coefficient of $Y_{1-x}Ca_xCoO_3$ in low temperature range $T < \sim 550$ K decreased remarkably with increasing Ca content. For instance, S at 400 K decreased from ~1020 $\mu V\,K^{-1}$ for x=0 to ~525 $\mu V\,K^{-1}$ for x=0.01, ~325 $\mu V\,K^{-1}$ for x=0.05, and then ~270 $\mu V\,K^{-1}$ for x=0.1. However, an interesting phenomenon one can find in Fig. 5 is the fact that Ca doping does not affect the high-temperature limit of Seebeck coefficient of $Y_{1-x}Ca_xCoO_3$, all approaching ~150 $\mu V/K$ as T reaches around 800 K. The phenomenon observed here is similar to that reported by Palstra *et al.*[37] and Kobayashi *et al.*[38] in $LaMnO_3$ and other manganites. Therefore, the total thermopower of $Y_{1-x}Ca_xCoO_3$ can be expressed as the sum of temperature independent term and temperature dependent term, that is,

$$S = S_0 + \frac{k_B}{|e|} \cdot \frac{E_S}{k_B T}, \tag{4}$$

where E_s is a characteristic energy for S and S_0 is the thermopower in high-temperature limit. It can be seen from formula (4) that the contribution of the second term on the right to the total thermopower decreases rapidly with increasing temperature. Furthermore, it is worthwhile to note that the characteristic energy E_s is an apparent parameter because it is not only a function of doping content (as found in other manganese oxides[37,38]) but also the (presumably decreasing) function of temperature since the semiconductor-metal transition is involved in $YCoO_3$ system at elevated temperatures ($T > \sim 550$ K),[26] which will cause the temperature dependent constituent to diminish much more rapidly than in manganites (in which there is no such transition occurring at the high temperatures). The thermopower S_0 in high-temperature limit may be related to degeneracy of electron configuration (spin and/or orbit) of Co ions in $YCoO_3$ system as suggested by Koshibae *et al.*,[39] and it could be described by extended Heikes formula written as

$$S_0 = -\frac{k_B}{e} \ln\left[\frac{g_3}{g_4}\frac{y}{1-y}\right], \tag{5}$$

where g_3 and g_4 are the number of the degenerated configuration of the Co^{3+} and Co^{4+} states, respectively; y (=Co^{4+}/Co) is the concentration of Co^{4+} holes on the Co sites. According to the valence-band photoemission study results by Mizokawa *et al.*[40] for (Bi,Sr)CoO_3, we could assume that the spin states of Co^{3+} and Co^{4+} exist in low spin state t_{2g}^6 and t_{2g}^5, respectively, and that the concentration ratio of Co^{3+} and Co^{4+} is 1:1, which gives g_3=1, g_4=6, and y=0.5. Substituting these values into formula (5), we obtained $S_0 \sim 154$ $\mu V\,K^{-1}$ (as predicted by Koshibae *et al.*[39]), which is in good agreement with experimental values of thermpower (~150 $\mu V\,K^{-1}$) at high temperatures ($T > 800$ K) for $YCoO_3$ system. Present result suggests that (1) Co ions (Co^{3+} and Co^{4+}) in $YCoO_3$ exist largely in low spin state even at the temperatures as high as 800 K, which implies that the semiconductor-metal transition could not be mainly attributed to the transition from low-spin (LS) to high-spin (HS) or intermediate-spin (IS) state of the Co ions, and (2) the contribution of increased concentration of Co^{4+} (caused by Ca doping) to S_0 is very limited. In other words, the increase of concentration of Co^{4+} mainly influences the temperature dependent term through increasing carrier (hole) concentration as discussed above. In fact, the decrease of thermopower for $Y_{1-x}Ca_xCoO_3$ in low temperature range $T < \sim 550$ K (in Fig. 5) with increasing carrier concentration (or with increase doping content of Ca) can be understood in terms of normal semiconductor band theory.[20,41]

2. Thermal conductivity

The temperature dependences of thermal conductivity κ for the $Y_{1-x}Ca_xCoO_3$ ($0 \leqslant x \leqslant 0.1$) compounds in the tem-

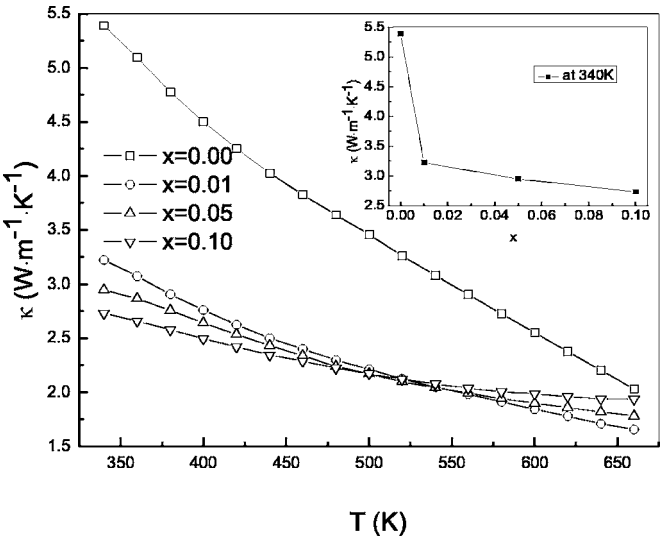

FIG. 6. Thermal conductivity κ as a function of temperature T for $Y_{1-x}Ca_xCoO_3$ ($x=0,0.01,0.05,0.1$). The inset shows the plot of κ vs Ca content x at 340 K for $Y_{1-x}Ca_xCoO_3$.

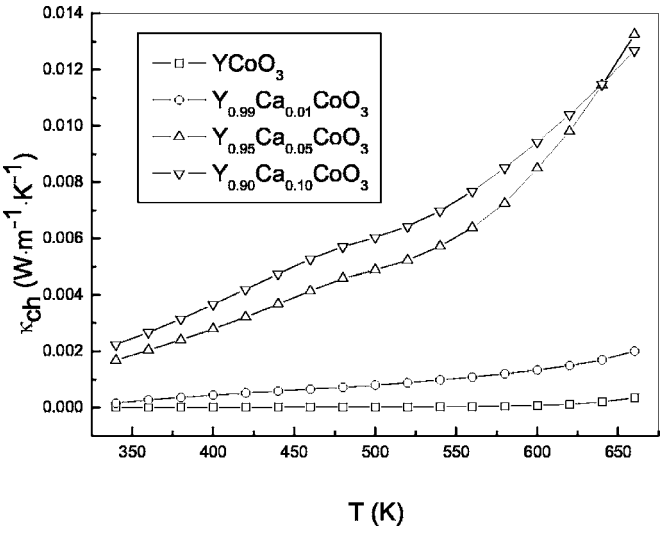

FIG. 7. Carrier thermal conductivity κ_{ch} as a function of temperature T for $Y_{1-x}Ca_xCoO_3$ ($x=0,0.01,0.05,0.1$).

perature range from 340 to 660 K are displayed in Fig. 6. The total thermal conductivity κ of $YCoO_3$ decreases almost linearly from 5.39 to 2.03 W m^{-1} K^{-1} with increasing temperature from 340 to 660 K. As compared to that of $YCoO_3$, the thermal conductivity of $Y_{1-x}Ca_xCoO_3$ ($x\neq 0$) becomes much smaller in the whole temperature range measured, though it also decreases monotonously with increasing temperature. For instance, the thermal conductivity of $Y_{0.99}Ca_{0.01}CoO_3$ decreases from 2.73 to 1.94 W m^{-1} K^{-1} with increasing temperature from 340 to 660 K. As the Ca content increases, the thermal conductivity decreases monotonously at the temperatures $T<\sim 520$ K, as shown in the inset of Fig. 6 that gives κ as a function of Ca content x at 340 K. However, we see that as $x>0.01$ the decrease of κ becomes slower with further increase of Ca content x, indicating that lighter doping is very effective in reducing thermal conductivity of $YCoO_3$. Here, one interesting phenomenon observed in Fig. 6 is that the thermal conductivity of more heavily doped samples decreases more slowly with increasing temperature, which causes plots of κ versus temperature T for all the doped $Y_{1-x}Ca_xCoO_3$ samples to cross at about 520 K, above which thermal conductivity of more heavily doped samples is larger that that of more lightly doped samples. This result indicates that too heavy doping is not very effective as, or even worse than, light doping in reducing thermal conductivity at $T>520$ K.

One notices that there are some discrepancies between present results for $YCoO_3$ and those previously reported by Hejtmanek *et al.*[27] The thermal conductivity ($\sim$1.5 W m^{-1} K^{-1} at 300 K) of $Y_{1-x}Ca_xCoO_3$ ($x=0$) obtained by them is obviously smaller than that obtained here. Furthermore, the measurements indicated that the thermal conductivity of the doped sample with $x=0.1$ is larger than that of undoped one ($x=0$) below room temperature, which seems to be difficult to understand. The reasons why the thermal conductivity of the doped sample is larger than that of the undoped one and why their measured thermal conductivity of $YCoO_3$ is smaller than that obtained here would originate from the differences in porosity content in their samples. As mentioned by them, the samples possessed high porosity (in contrast, our samples all have high relative densities around 88%–90%) that will make the apparent thermal conductivity be much lower, and if the porosity content was not well controlled among samples the comparison of the thermal conductivity of the doped sample with that of the undoped one is unreliable and intrinsically meaningless.

The overall thermal conductivity of a solid generally consists of two-part contribution: lattice thermal conductivity κ_l and mobile charge-carrier thermal conductivity κ_{ch}, i.e., $\kappa=\kappa_l+\kappa_{ch}$, where κ_{ch} can be estimated by the Wiedemann-Franz law, $\kappa_{ch}=LT/\rho$ [L, the Lorentz number (2.45 $\times 10^{-8}$ V^2 K^{-1} for free electrons)]. Figure 7 presents the charge carrier thermal conductivity κ_{ch}, estimated using the Wiedemann-Franz law, of $Y_{1-x}Ca_xCoO_3$ as a function of temperature T (340–660 K). One can see with increasing Ca content of substitution the carrier thermal conductivity κ_{ch} of $Y_{1-x}Ca_xCoO_3$ becomes larger. For instance, at $\sim$340 K the carrier conductivity increase from 3.48×10^{-6} W m^{-1} K^{-1} for $x=0$ to 1.51×10^{-4} W m^{-1} K^{-1} for $x=0.01$; then it increases to 2.23×10^{-3} W m^{-1} K^{-1} for $x=0.1$. This increase of κ_{ch} could be ascribed to the increase of carrier concentration. Moreover, κ_{ch} for all $Y_{1-x}Ca_xCoO_3$ compounds increases monotonically with increasing temperature. Especially, κ_{ch} for more heavily doped samples increases much faster than that of less heavily doped samples as temperature increases. This phenomenon suggests that much slower decrease of κ with increasing temperature (Fig. 6) for heavy doped samples would be caused by the increased contribution coming from carriers at higher temperatures. Nevertheless, the ratio of carrier contribution (κ_{ch}) to total thermal conductivity is quite small. For instance, at 600 K the ratio κ_{ch}/κ is 0.0030% for $x=0$, 0.072% for $x=0.01$, 0.448% for $x=0.05$, and 0.474% for $x=0.1$. This indicates that the overall thermal conductivity of $Y_{1-x}Ca_xCoO_3$ comes mainly from the lattice thermal conductivity, as found in similar system[42,43] $(Gd,Sm,Nd,Pr,Ho)CoO_3$. In other words, Ca substitution leads to substantial decrease (38.7% and 44.7% at 400 K for

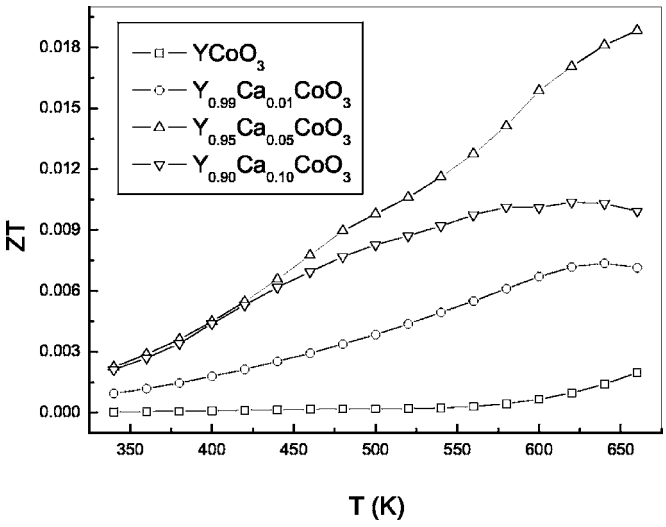

FIG. 8. Dimensionless figure of merit ZT as a function of temperature T for $Y_{1-x}Ca_xCoO_3$ ($x=0, 0.01, 0.05, 0.1$).

$x=0.05$ and 0.10, respectively) of lattice thermal conductivity of $Y_{1-x}Ca_xCoO_3$. This decrease in κ_l could be attributed to the reduction in mean free path of the phonons due to increased impurity (doped Ca) scattering. However, the enhancement of sound velocity of heavily doped samples would become pronounced because of the atomic weight of Ca being smaller than that of Y, which could explain why heavy doping is not as effective as light doping in suppressing the thermal conductivity.

3. Figure of merit

The temperature dependences of the dimensionless figure-of-merit ZT $[=S^2T/(\rho\kappa)]$ for $Y_{1-x}Ca_xCoO_3$ ($0 \leqslant x \leqslant 0.1$) compounds in the temperature range from 340 to 660 K are shown in Fig. 8. One can see that for the undoped $Y_{1-x}Ca_xCoO_3$ sample ($x=0$) its ZT is very small in the whole temperature investigated, and largest magnitude of its ZT is about 0.0020 (at 660 K). This small ZT value lies in the fact that although $YCoO_3$ has very large thermopower, its electric resistivity and thermal conductivity are relatively very high, which makes its ZT be very small. As $Y_{1-x}Ca_xCoO_3$ is doped with 1% of Ca ($x=0.01$), its ZT is improved substantially with largest value being around 0.0074 (at 640 K) because of large decrease in both its resistivity and its thermal conductivity. Particularly, ZT of the $Y_{1-x}Ca_xCoO_3$ sample with $x=0.05$ is the best with largest value being $\sim$0.019 (at 660 K) that is about tenfold greater than that of the pristine compound. However, one notices that ZT for the heavily doped $Y_{1-x}Ca_xCoO_3$ sample with $x=0.1$ declines in the whole temperature range investigated as compared to the sample with $x=0.05$, which results from the fact that its thermopower decreases obviously, while its electrical resistivity and thermal conductivity do not decrease very much as compared to the sample with $x=0.05$. Present results indicate that proper substitution of Ca for Y in $YCoO_3$ can remarkably improve its high-temperature thermoelectric properties.

IV. CONCLUSION

The electrical transport and thermoelectric properties of $Y_{1-x}Ca_xCoO_3$ ($0 \leqslant x \leqslant 0.1$) were investigated in the temperature range from 300 to 780 K. The results indicated that dc resistivity of $Y_{1-x}Ca_xCoO_3$ all decreased remarkably with increasing Ca content x, which could be explained as increase of hole concentration. The temperature dependences of the resistivity for $Y_{1-x}Ca_xCoO_3$ were all found to be basically consistent with small-polaron hopping conduction model with activation energy for conduction decreasing with increase of doping content. Although the thermopower of $Y_{1-x}Ca_xCoO_3$ at low temperatures $T < \sim 550$ K decreased remarkably with increasing Ca content x, it approached a limit value of $S_0 \sim 150$ μV/K at $\sim$800 K for all the samples with different x, which was consistent well with the estimated value from Heikes formula assuming that Co^{3+} to Co^{4+} exist in low spin state. Experiments showed that thermal conductivity of $Y_{1-x}Ca_xCoO_3$ came mainly from its lattice component, and its decrease could be chiefly attributed to impurity (doped Ca) scattering. It was found that ZT of $Y_{1-x}Ca_xCoO_3$ changed nonmonotonously with increasing doping content of Ca, and $Y_{0.95}Ca_{0.05}CoO_3$ had optimum thermoelectric properties with $ZT=0.019$ at 660 K, which was about tenfold greater than that of $YCoO_3$, indicating that its thermoelectric properties could be improved substantially by proper substitution of Ca for Y in this compound.

ACKNOWLEDGMENTS

This work is financially supported by National Natural Science Foundation of China under Contract Nos. 50371081 and 50472097.

[1] I. Matsubara, R. Funahashi, T. Takeuchi, S. Sodeoka, T. Shimizu, and K. Ueno, Appl. Phys. Lett. **78**, 3627 (2001).
[2] W. Shin, N. Murayama, K. Ikeda, and S. Sago, J. Power Sources **103**, 80 (2001).
[3] G. Xu, R. Funahashi, M. Shikano, I. Matsubara, and Y. Zhou, Appl. Phys. Lett. **80**, 3760 (2002).
[4] R. Funahashi and M. Shikano, Appl. Phys. Lett. **81**, 1459 (2002).
[5] G. Xu, R. Funahashi, M. Shikano, I. Matsubara, and Y. Zhou, J. Appl. Phys. **91**, 4344 (2002).
[6] A. Maignan, S. Hébert, L. Pi, D. Pelloquin, C. Martin, C. Michel, M. Hervieu, and B. Raveau, Cryst. Eng. **5**, 365 (2002).
[7] G. S. Nolas, J. Sharp, and H. J. Goldsmid, *Thermoelectrics: Basic Principles and New Materials Developments*, 1st ed. (Springer-Verlag, Germany, 2001), p. 8.
[8] C. M. Bhandari and D. M. Rowe, *CRC Handbook of Thermoelectrics* (CRC, London, 1995).
[9] I. Terasaki, Y. Sasago, and K. Uchinokura, Phys. Rev. B **56**, R12685 (1997).
[10] A. C. Masset, C. Michel, A. Maignan, M. Hervieu, O. Toulemonde, F. Studer, and B. Raveau, Phys. Rev. B **62**, 166 (2000).
[11] S. Li, R. Funahashi, I. Matsubara, K. Ueno, S. Sodeoka, and H. Yamada, Chem. Mater. **12**, 2424 (2000).
[12] B. Fisher, L. Patlagan, G. M. Reisner, and A. Knizhnik, Phys. Rev. B **61**, 470 (2000).
[13] D. Li, X. Y. Qin, Y. J. Gu, and J. Zhang, Solid State Commun. **134**, 235 (2005).
[14] A. Maignan, S. Hebert, D. Pelloquin, and C. Michel, J. Appl. Phys. **92**, 1964 (2002).
[15] J. Nan, J. Wu, Y. Deng, and C.-W. Nan, Solid State Commun. **124**, 243 (2002).
[16] I. Matsubara, R. Funahashi, T. Takeuchi, and S. Sodeoka, J. Appl. Phys. **90**, 462 (2001).

[17]D. Wang, L. Chen, Q. Yao, and J. Li, Solid State Commun. **129**, 615 (2004).
[18]G. Xu, R. Funahashi, M. Shikano, I. Matsubara, and Y. Zhou, Appl. Phys. Lett. **80**, 3760 (2002).
[19]S. Li, R. Funahashi, I. Matsubara, H. Yamada, K. Ueno, and S. Sodeoka, Ceram. Int. **27**, 321 (2001).
[20]J. Androulakis, P. Migiakis, and J. Giapintzakis, Appl. Phys. Lett. **84**, 1099 (2004).
[21]A. Maignan, D. Flahaut, and S. Hébert, Eur. Phys. J. B **39**, 145 (2004).
[22]V. G. Bhide, D. S. Rajoria, Y. S. Reddy, G. Rama Rao, and C. N. R. Rao, Phys. Rev. B **8**, 5028 (1973).
[23]K. Knížek, Z. Jirák, J. Hejtmánek, M. Veverka, M. Maryško, G. Maris, and T. T. M. Palstra, Eur. Phys. J. B **47**, 213 (2005).
[24]G. Demazeau, M. Pouchard, and P. Hagenmuller, J. Solid State Chem. **9**, 202 (1974).
[25]A. Mehta, R. Berliner, and R. W. Smith, J. Solid State Chem. **130**, 192 (1997).
[26]G. Thornton, F. C. Morrison, S. Partington, B. C. Tofield, and D. E. Williams, J. Phys. C **21**, 2871 (1988).
[27]J. Hejtmánek, K. Knížek, and H. Fujishiro, Proceedings of 2nd European Conference on Thermoelectrics (8th European Workshop on Thermoelectrics) of European Thermoelectric Society, Poland, Kraków, 2004, No. 24, http://home.agh.edu.pl/~ets2004/proceedings/proceedings.htm.
[28]J. Hejtmánek, Z. Jirák, K. Knížek, M. Maryško, M. Veverka, and H. Fujishiro, J. Magn. Magn. Mater. **272**, e283 (2004).
[29]Y. Liu and X. Y. Qin, J. Phys. Chem. Solids **67**, 1893 (2006).
[30]V. M. Goldsmit, Geochemische Vertailungsgesetze der Elemente, Skrifter Norske Videnskaps-Akad. Oslo I Mat-Naturr. **2**, 7 (1926).
[31]T. He, J. Z. Chen, T. G. Calvarese, and M. A. Subramanian, Solid State Sci. **8**, 467 (2006).
[32]N. F. Mott and H. Jones, *The Theory of the Properties of Metals and Alloys* (Dover, New York, 1958), p. 305.
[33]G. Ch. Kostogloudis, N. Vasilakos, and Ch. Ftkos, Solid State Ionics **106**, 207 (1998).
[34]F. A. Kröger and H. J. Vink, *Solid State Physics Advances in Research and Applications* (Academic, New York, 1957), p. 307.
[35]A. Mineshige, M. Kobune, S. Fujii, Z. Ogumi, M. Inaba, T. Yao, and K. Kikuchi, J. Solid State Chem. **142**, 374 (1999).
[36]M. Itoh, J. Hashimoto, S. Yamaguchi, and Y. Tokura, Physica B **281&282**, 510 (2000).
[37]T. T. M. Palstra, A. P. Ramirez, S.-W. Cheong, B. R. Zegarski, P. Schiffer, and J. Zaanen, Phys. Rev. B **56**, 5104 (1997).
[38]W. Kobayashi, I. Terasaki, M. Mikami, R. Funahashi, T. Nomura, and T. Katsufuji, J. Appl. Phys. **95**, 6825 (2004).
[39]W. Koshibae, K. Tsutsui, and S. Maekawa, Phys. Rev. B **62**, 6869 (2000).
[40]T. Mizokawa, L. H. Tjeng, and P. G. Steeneken, Phys. Rev. B **64**, 115104 (2001).
[41]P. S. Kireev, *Semiconductor Physics*, 2nd ed. (MIR, Moscow, 1978), p. 324.
[42]J.-W. Moon, W.-S. Seo, H. Okabe, T. Okawa, and K. Koumoto, J. Mater. Chem. **10**, 2007 (2000).
[43]J.-W. Moon, Y. Masuda, W.-S. Seo, and K. Koumoto, Mater. Lett. **48**, 225 (2001).